

AN INVESTIGATION OF MULTIPLE-DISK
TURBINE PERFORMANCE PARAMETERS

by

Michael John Lawn, Jr.

has been approved

January 1972

APPROVED:

Warren Rice, Chairman
Earl J. ...
R. L. Mitzelworth
...

Supervisory Committee

ACCEPTED:

John F. Beggs
Department Chairman
...
Dean, Graduate College

ABSTRACT

Using an earlier developed mathematical model applicable for laminar flow of an incompressible Newtonian fluid, radially inward between parallel co-rotating disks, performance curves for an unconventional type of turbomachinery are presented. Parabolic and uniform input velocity profiles with full admission of the working fluid to the rotor is assumed. Performance data for the general flow problem require that three dimensionless input parameters be specified, a Reynolds number, a flow rate parameter, and a peripheral tangential velocity component parameter. The output of the mathematical model is the dimensionless characteristics torque, total pressure, and efficiency at specified radial locations.

Using this output data individual performance characteristics are plotted, functions of the Reynolds number and the flow rate parameter. Each is a separate constant value curve for a specified exit radial location and peripheral tangential velocity parameter. Composite maps are also presented showing the characteristics of all three parameters on a single graph.

An example is presented which shows how the performance maps are used. Using three different working fluids the results, in dimensional quantities, indicate the specifications and characteristics of a multiple-disk turbine.

All results in this study are for a mathematical model having no losses external to the turbine rotor. The performance maps show, however, that the multiple-disk turbine is competitive with conventional bladed turbines in areas of power generation where low horsepower and high speeds are required.

ACKNOWLEDGMENTS

The author would like to acknowledge the individuals who have given guidance and encouragement during the course of this study. Dr. Warren Rice acted as chairman of the supervisory committee, suggested the thesis topic, and offered timely suggestions which aided the author in his investigation. Appreciation is also expressed to the following professors who served on the author's graduate committee: Dr. Earl Logan and Dr. Richard Ditsworth.

Finally, appreciation is extended to Michael Crawford, who took time during his own course of study to help the author with computer programming problems that arose during this study.

TABLE OF CONTENTS

	Page
LIST OF FIGURES	viii
NOMENCLATURE	x
 Chapter	
I. INTRODUCTION	1
CONVENTIONAL TURBOMACHINERY.	1
UNCONVENTIONAL TURBOMACHINERY.	2
BACKGROUND	4
II. MULTIPLE-DISK TURBINE ANALYSIS	9
PRESENT STATUS OF ANALYSIS	9
SUMMARY OF BOYACK'S ANALYSIS	10
TURBINE PERFORMANCE PARAMETERS	20
III. PERFORMANCE MAPS	22
BOYACK'S COMPUTED RESULTS.	22
GRAPHICAL METHODS.	23
GENERAL CURVE CHARACTERISTICS.	25
LIMITATIONS.	31
DESIGN CHARACTERISTICS	33
IV. CONCLUSION	47
SUMMARY.	47

Chapter	Page
RECOMMENDATIONS.	48
FURTHER STUDY.	48
REFERENCES	50
APPENDIX A: MODIFIED BOYACK PROGRAM	53
APPENDIX B: BOYACK OUTPUT DATA SHEETS	92
APPENDIX C: PERFORMANCE MAPS.	100
1. PERFORMANCE MAPS. PLOTTED FOR $V_0 = 1.0$ WITH PARABOLIC INLET PROFILES.	101
2. PERFORMANCE MAPS. PLOTTED FOR $V_0 = 1.1$ WITH PARABOLIC INLET PROFILES.	129
3. PERFORMANCE MAPS. PLOTTED FOR $V_0 = 1.3$ WITH PARABOLIC INLET PROFILES.	158
4. COMPOSITE MAPS. PLOTTED FOR $V_0 = 1.1$ WITH PARABOLIC INLET PROFILES	186
5. PERFORMANCE GRAPHS	195
6. PERFORMANCE MAPS. PLOTTED FOR $V_0 = 1.1$ WITH UNIFORM INLET PROFILES.	214
APPENDIX D: DESIGN PROGRAM.	241
APPENDIX E: DESIGN PROGRAM OUTPUT SHEETS.	245

LIST OF FIGURES

Figure	Page
I-1. Schematic Diagram of Turbine Using a Disk Rotor.	3
I-2. A Typical Multiple-Disk Rotor.	5
II-1. Definition of Reference Coordinate System.	11
III-1. Typical Map of Turbine Efficiency as a Function of U_0 and N_{RE} for $V_0 = 1.1$, $R_i = 0.3$ and Parabolic Inlet.	26
III-2. Typical Map of Turbine Dimensionless Torque as a Function of U_0 and N_{RE} for $V_0 = 1.1$, $R_i = 0.3$ and Parabolic Inlet	27
III-3. Typical Map of Turbine Dimensionless Total Pressure as a Function of U_0 and N_{RE} , for $V_0 = 1.1$, $R_i = 0.3$ and Parabolic Inlet	23
III-4. Composite Map Showing η , T , and PT as a Function of U_0 and N_{RE} for $V_0 = 1.1$, $R_i = 0.3$ and Parabolic Inlet	29
III-5. Plot of RPM and Torque Versus Density with Head = 200 Feet.	36
III-6. Plot of RPM, Disk Spacing, and Torque Versus Head for Liquid Hydrogen and Outer Rotor Radius = 4.0 Inches.	38
III-7. Plot of RPM, Disk Spacing, and Torque Versus Head for Liquid Sodium and Outer Rotor Radius = 4.0 Inches.	39
III-8. Plot of RPM, Disk Spacing, and Torque Versus Head for Glycerine and Outer Rotor Radius = 4.0 Inches.	40
III-9. Plot of RPM, Disk Spacing, and Torque Versus Outer Rotor Radius for Liquid Hydrogen for Head = 200 Feet.	41

Figure	Page
III-10. Plot of RPM, Disk Spacing, and Torque Versus Outer Rotor Radius for Liquid Sodium for Head = 200 Feet.	42
III-11. Plot of RPM, Disk Spacing, and Torque Versus Outer Rotor Radius for Glycerine for Head = 200 Feet.	43
III-12. Illustration of Off-Design-Point Operation for Liquid Hydrogen. Design $R_0 = 2.0$ Inches and Head = 200 Feet.	44
III-13. Illustration of Off-Design-Point Operation for Liquid Sodium. Design $R_0 = 4.0$ Inches and Head = 200 Feet.	45
III-14. Illustration of Off-Design-Point Operation for Glycerine. Design $R_0 = 10.0$ Inches and Head = 200 Feet.	46

NOMENCLATURE

$a = a(r)$	coefficient in polynomial, (dimensionless)
$b = b(r)$	coefficient in polynomial, (dimensionless)
E_K	calculated truncation error
\bar{h}	distance between disks, (length)
N	order of polynomial, (integer)
$N_{RE} = \frac{\rho \bar{h}^2 \Omega}{\mu}$	Reynolds number (dimensionless)
\bar{p}	pressure, (force/area)
$P, p = \frac{\bar{p}}{\rho \bar{r}_0^2 \Omega^2}$	pressure, (dimensionless)
\overline{PT}	total pressure, (force/area)
PT, p_t	total pressure, (dimensionless)
Q	volume flow rate, (volume/time)
\bar{R}, \bar{r}	radius, (length)
$R, r = \frac{\bar{r}}{\bar{r}_0}$	radius, (dimensionless)
T_s, T	torque, (dimensionless)
\bar{T}	torque, (length-force)
\bar{u}	radial component of velocity, (length/time)
$u = \frac{\bar{u}}{\bar{r}_0 \Omega}$	radial component of velocity, (dimensionless)
$U_0 = 2 \int_0^{1/2} u(1,z) dz$	dimensionless flow rate parameter

\bar{v}	tangential component of velocity, (length/time)
$v = \frac{\bar{v}}{\bar{r} \Omega}$	tangential component of velocity, (dimensionless)
$V_0 = 2 \int_0^{1/2} v(l,z) dz$	dimensionless tangential velocity parameter
\bar{w}	axial component of velocity, (length/time)
$w = \frac{\bar{w}}{\bar{h} \Omega}$	axial component of velocity, (dimensionless)
\bar{z}	axial coordinate, (length)
$z = \frac{\bar{z}}{\bar{h}}$	axial coordinate, (dimensionless)
Ω	angular velocity of disks, (rad/time)
ρ	fluid density, (mass/length ³)
μ	viscosity, (force-time/length ²)
η	turbine efficiency
ν	kinematic viscosity, (length ² /time)
α	nozzle angle, (deg)
β, ξ	dummy variables

Subscripts

i	inner radius of disks
o	outer radius of disks

Chapter I

INTRODUCTION

CONVENTIONAL TURBOMACHINERY

Conventional turbomachinery utilizes the energy of the working fluid to develop pressure, reaction, or impact forces on a series of blades or vanes. The blades are generally airfoil shapes, elaborately contoured, and precision machined to specifications determined by design operating conditions to induce maximum momentum transfer with minimum energy losses.

Methods of analysis used for aircraft wings can be applied to study the fluid flow past conventional turbine blades. The flow between adjacent blades is complicated and exact solutions of the governing equations for the flow process are complex, and a viscous flow analysis is difficult. The viscous effects are, therefore, usually ignored in analytical work, reducing the problem to an analysis of inviscid flow past an airfoil. Empirical correction factors are introduced later to account for viscous effects.

The losses due to viscous shear forces become severe as the diameter of bladed rotors and blade spacing decrease. As the turbine size is reduced the volume flow rate of the working fluid is reduced, therefore there is a reduction in specific speed and efficiency. As a

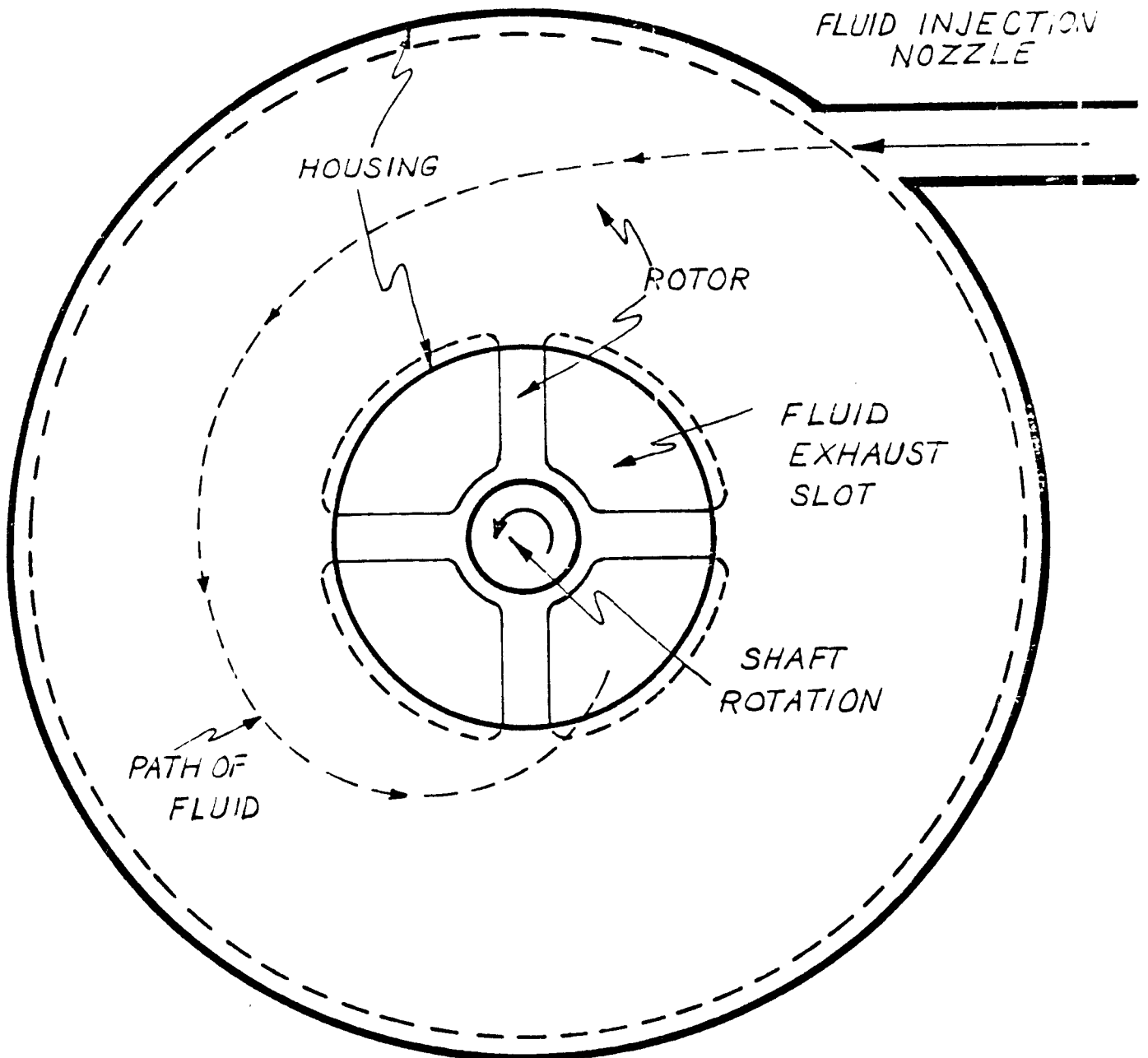
result conventional bladed turbines have low efficiencies in situations requiring high energy transfer with small volume flow rates. The primary advantage of bladed turbines is a high power output-to-weight ratio and high efficiencies for large units.

UNCONVENTIONAL TURBOMACHINERY

One type of unconventional turbomachinery uses fluid viscous effects as a mechanism for the transfer of energy. The rotor consists of a series of flat, circular disks mounted parallel on a shaft. The disks are attached at small intervals along the shaft, and each disk has an opening at an inner radius for the exhaust of the fluid. The rotor is enclosed with a housing which contains a stator to provide the working fluid with a velocity vector that is nearly tangential relative to the outer periphery of disks. As the fluid element moves in a spiral path to the exhaust port, the viscous shear effects, in the tangential direction, tend to draw the disks along in the same direction of the flow. A schematic diagram of the fluid flow is represented in Figure I-1.

Since the geometry of the disk turbine is simple a number of analytical and numerical approaches can be used in the flow analysis. Any analysis, however, must include the viscous properties of the fluid since this property provides the motive power for the multiple-disk turbine.

The disk turbine has several inherent advantages. Construction costs are relatively low because disks can be produced in large quantities from a stamp press; extensive precision machinery is not required.



HOUSING SUPPORT, ROTOR BEARINGS AND BEARING SUPPORTS, AND ROTOR TO HOUSING SEALS OMITTED FOR CLARITY.

Figure I-1. Schematic Diagram of Turbine Using a Disk Rotor

Maintenance can be held to a minimum due to the simplicity of the device and the ease of replacing damaged or worn disks. The disk turbine also allows high operating temperatures to be maintained without structural failure. A wide range of working fluids is also possible. The primary advantage of the multiple-disk turbine is its ability to produce low horsepower, with high efficiency at high speeds, with a very low noise level. A typical disk rotor is presented in Figure I-2.

BACKGROUND

The development of multiple-disk turbomachinery dates from the turn of the century to the present. Nikola Tesla was granted the U.S. Patent covering both multiple-disk turbines and pumps in 1913 [1]. In his patent application, Tesla described the motive forces of his machinery as being dependent on the fluid properties of viscosity and adhesion. Several successful turbines were designed and built by Tesla [2,3] but they were considered not commercially feasible at the time. Lack of adequate materials, difficulties in handling inherent high speeds, and heat dissipation problems were the reasons for multiple disk devices not being further developed.

In the succeeding years a number of experimental and analytical investigations confirmed the feasibility of multiple-disk turbomachinery [4-11]. Since 1955 qualitative analyses have been published which used either hydraulic friction factor, empirical information, or assumed velocity distributions to estimate performance [12-16]. Although these results are not sufficient for design studies, they confirm the feasibility of multiple-disk devices.

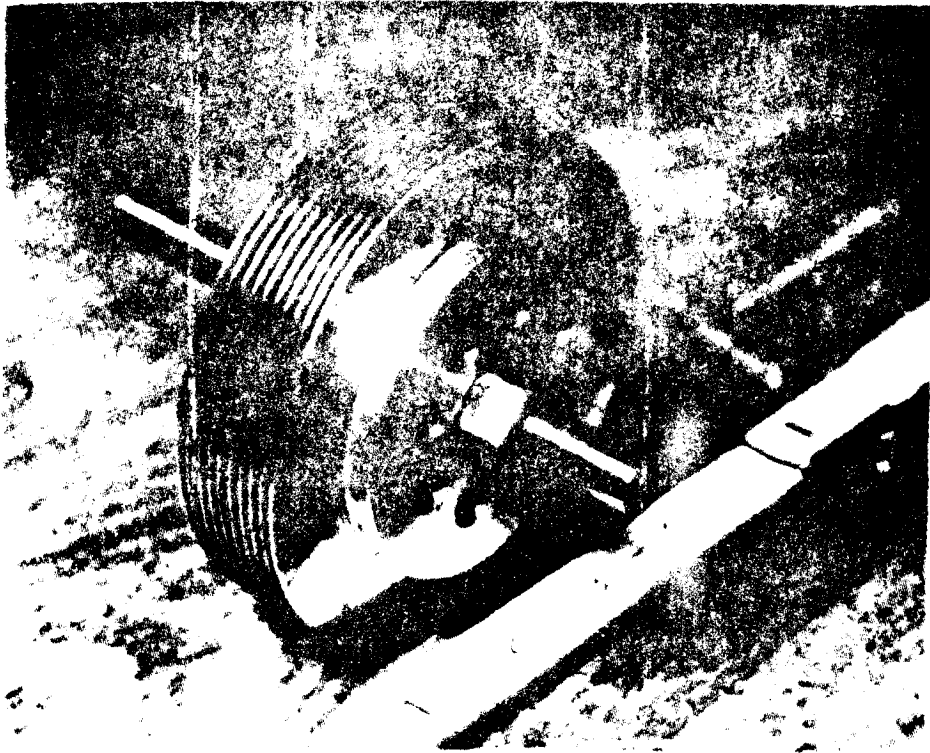


Figure 1-2. A Typical Microble-Of...

In 1962 Breiter and Pohlhausen [17] presented rigorous approach to laminar flow of a viscous, incompressible fluid between two parallel rotating disks operating as a multiple-disk pump. By assuming a very small through-flow rate they linearized the governing Navier-Stokes equations and obtained a similarity solution. Near the inlet the linearized equations did not apply, and it was necessary to solve the non-linear equations numerically. The solution of the linearized governing equations, valid for small flow rates and radial stations well removed from the entrance region, describes the asymptotic flow field. The solution of the non-linear equations represents realistic inlet conditions and is useful for the radially outward flow case.

An investigation by Matsch [18] in 1967 considered radially inward flow between rotating disks, which models the multiple-disk turbine. Reduced Navier-Stokes equations were solved, for both partial and full admission of fluid, by an iterative method. The first approximation was the solution to the linearized form of the governing equations. The second order approximation was obtained from the discarded non-linear terms using the results of the first approximation. The procedure was repeated until convergence was obtained, and a functional solution through the third approximation was found. The solution only specified the dimensionless volume flow rate and Reynolds number as parameters, resulting in an insufficient number of parameters compared to the number needed for a general solution. The results are only valid for the asymptotic flow region occurring at a radial station interior to the inlet region. The asymptotic solution does not provide sufficient information for the calculation of actual turbine performance.

A sufficiently complete problem statement was formulated from the Navier-Stokes equations by Boyd [19,20] for radially inward flow between rotating disks. Boyd introduced a third parameter, a peripheral tangential velocity component, which may be greater or less than the disk peripheral velocity. The reduced Navier-Stokes equations were solved for full admission of the working fluid, and an inverse finite-difference technique was used to obtain a numerical solution to the problem statement. The solution becomes the asymptotic solution at interior radii, and is in full agreement with Matsch [18]. The solution was the first of sufficient generality to allow the analysis of turbine performance over a wide range of flow parameters.

Adams [21] conducted an experimental investigation which was useful in the testing of theory. The test fixture consisted of two narrowly spaced disks which were attached to a shaft. The housing included supply nozzles which approximated the full admission of fluid at the outer periphery. The static pressure distribution was measured for the following ranges of the flow governing parameters:

$$1.75 < N_{RE} < 8.25$$

$$- 0.50 < U_o < - 0.085$$

$$0.25 < V_o < 1.75$$

where N_{RE} is a Reynolds number and

$$U_o = 2 \int_0^{1/2} u(1,z) dz \quad (I-1)$$

$$V_0 = 2 \int_0^{1/2} v(1,z) dz . \quad (I-2)$$

U_0 and V_0 are the mean values of the radial and tangential velocities at the outer periphery of the disks.

The experimental and calculated pressure distributions compared well with the greatest divergence noted for $N_{RE} > 6.0$. Boyack [22] indicates that divergence of results at high Reynolds numbers may be due to order-of-magnitude reduced governing equations becoming less representative of the actual flow. Other investigators [15,19,20] have suggested that the onset of turbulent flow exists in the region. However no evidence of turbulent flow was found by Adams for the ranges of U_0 , V_0 , and N_{RE} investigated.

In 1969 Boyack [22] developed an integral method for the three-dimensional, non-boundary-layer flow, which occurs for laminar incompressible Newtonian fluid between co-rotating disks. Boyack's results agree very closely with the results obtained by Boyd's finite-difference method [19] and Adams' experiment [21].

Chapter II

MULTIPLE-DISK TURBINE ANALYSIS

PRESENT STATUS OF ANALYSIS

The general laminar flow of an incompressible, viscous fluid between co-rotating disks is described by the Navier-Stokes equations, subject to the no-slip boundary conditions at the disk surfaces. The fluid may be supplied at the outer periphery in many ways. Matsch and Rice [23,24] obtained solutions for the limiting cases of potential flow and creeping flow between co-rotating disks with partial admission at their outer periphery. Using order of magnitude arguments to simplify the governing equations, Matsch [18] obtained an iterative solution for the asymptotic flow field, with full admission.

The asymptotic solution, however, is not sufficient for the calculation of actual turbine performance, because the asymptotic flow usually occurs radially inward and away from the entrance. Boyd [19] formulated a sufficiently complete problem statement which included the entrance region as well as the asymptotic flow. The numerical method of solution as presented by Boyd is sufficiently accurate to calculate parameters such as torque, power, and efficiency for the rotors of multiple-disk turbines.

Boyd's numerical procedure [19], although accurate, is not efficient with regard to time needed on a digital computer to calculate

numerous flow cases for the plotting of performance maps. Boyack [22] developed an integral solution for the same problem presented in reference [19], which is accurate and efficient. The computation time, on the digital computer, of the Boyack integral method is one-fiftieth (1/50) of that required by the Boyd numerical procedure.

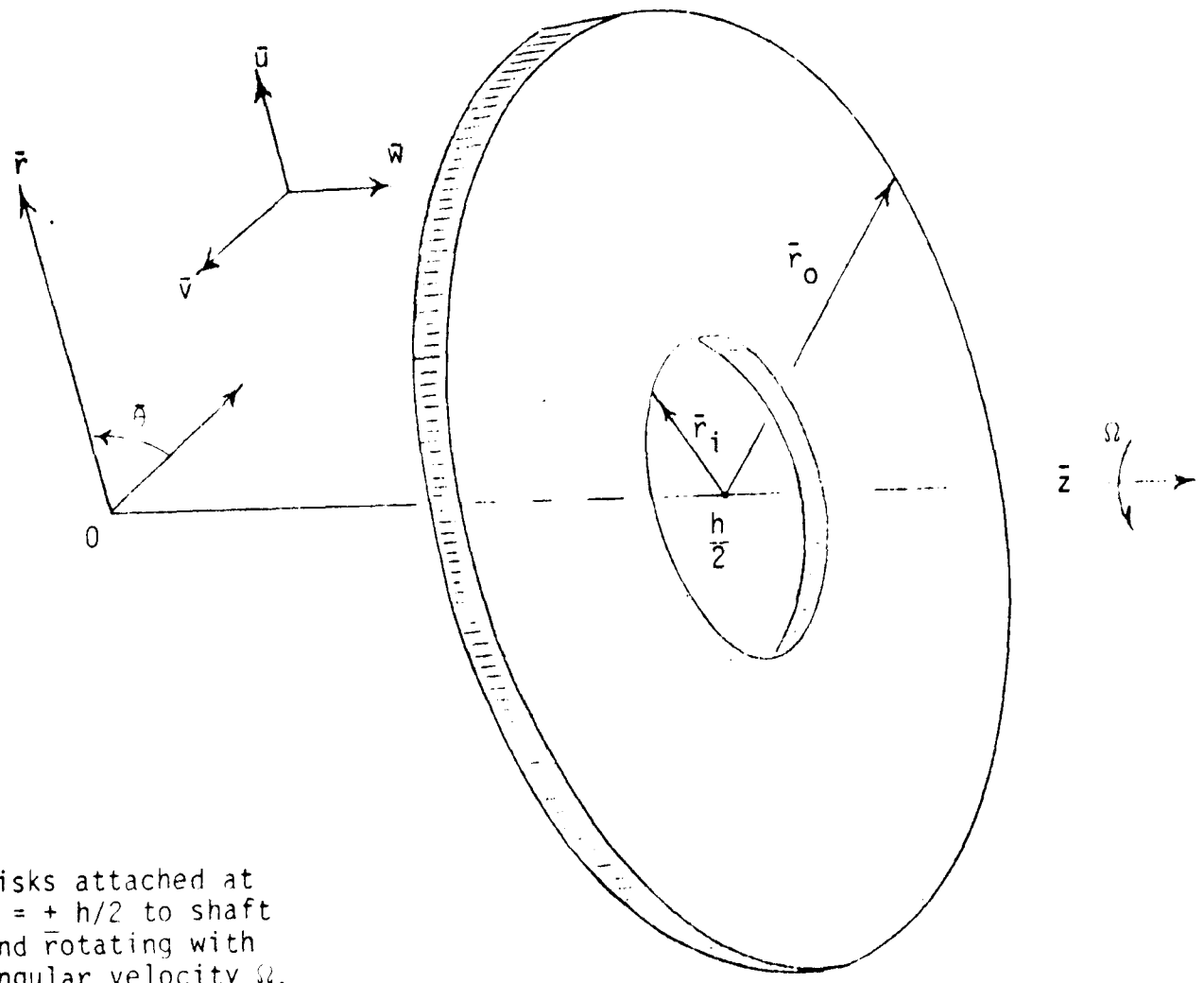
SUMMARY OF BOYACK'S ANALYSIS [22]

The solution presented by Boyack is necessary for the mapping of disk rotor performance for full admission, incompressible, laminar flow fields. The method is a forward-stepping procedure which satisfies the integrals of the governing differential equations, boundary conditions, and governing differential equations at every radius.

The Navier-Stokes equations are sufficiently general to describe the laminar flow of a Newtonian fluid. With the continuity equation the result is four general flow equations. The following assumptions are made:

1. constant viscosity of the working fluid,
2. constant density of the working fluid,
3. steady flow,
4. negligible body forces,
5. full admission of the working fluid at the outer periphery of the disks.

Using the coordinate system shown in Figure II-1, and de-dimensionalizing the momentum and continuity equations they become



Disks attached at $z = + h/2$ to shaft and rotating with angular velocity Ω . Shown is disk at $+ h/2$.

Figure II-1. Definition of Reference Coordinate System

$$\frac{u\partial u}{\partial r} + \frac{w\partial u}{\partial z} - \frac{v^2}{r} = -\frac{\partial p}{\partial r} + \frac{1}{N_{RE}} \left[\frac{\partial^2 u}{\partial r^2} + \frac{1}{r} \frac{\partial u}{\partial r} - \frac{\partial u}{\partial r} - \frac{u}{r^2} + \frac{\partial^2 u}{\partial z^2} \right] \quad (\text{II-1})$$

$$\frac{u\partial v}{\partial r} + \frac{w\partial v}{\partial z} + \frac{uv}{r} = \frac{1}{N_{RE}} \left[\frac{\partial^2 v}{\partial r^2} + \frac{1}{r} \frac{\partial v}{\partial r} - \frac{v}{r^2} + \frac{\partial^2 v}{\partial z^2} \right] \quad (\text{II-2})$$

$$\frac{u\partial w}{\partial r} + \frac{w\partial w}{\partial z} = -\frac{\partial p}{\partial r} + \frac{1}{N_{RE}} \left[\frac{\partial^2 w}{\partial r^2} + \frac{1}{r} \frac{\partial w}{\partial r} + \frac{\partial^2 w}{\partial z^2} \right] \quad (\text{II-3})$$

$$\frac{\partial u}{\partial r} + \frac{u}{r} + \frac{\partial w}{\partial z} = 0 \quad (\text{II-4})$$

where

$$N_{RE} = \frac{\rho \bar{h}^2 \Omega}{\mu} \quad (\text{II-5})$$

Using the order-of-magnitude arguments presented by Matsch [18], $h \ll \bar{r}_0$, equations (II-1), (II-2), (II-3), and (II-4) reduce to

$$\frac{u\partial u}{\partial r} + \frac{w\partial u}{\partial z} - \frac{v^2}{r} = -\frac{\partial p}{\partial r} + \frac{1}{N_{RE}} \frac{\partial^2 u}{\partial z^2} \quad (\text{II-6})$$

$$\frac{u\partial v}{\partial r} + \frac{w\partial v}{\partial z} + \frac{uv}{r} = \frac{1}{N_{RE}} \frac{\partial^2 v}{\partial z^2} \quad (\text{II-7})$$

$$\frac{\partial p}{\partial z} \approx 0 \quad (\text{II-8})$$

$$\frac{\partial u}{\partial r} + \frac{u}{r} + \frac{\partial w}{\partial z} = 0 \quad (\text{II-9})$$

The pressure can be assumed to be a function of the radial coordinate only.

If entrance, exhaust, and boundary conditions are assumed symmetric about the $r - \theta$ plane midway between the disks, they are

$$\begin{aligned} u(1,z) &= u_0(z) \\ v(1,z) &= v_0(z) \quad 0 \leq z \leq 1/2 \\ p(r_i, z) &= 0 \end{aligned} \quad (\text{II-10})$$

$$\begin{aligned} \frac{\partial u}{\partial z}(r,0) &= 0 & u(r,1/2) &= 0 \\ \frac{\partial v}{\partial z}(r,0) &= 0 & v(r,1/2) &= r \quad r_i \leq r \leq 1 \\ w(r,0) &= 0 & w(r,1/2) &= 0 \end{aligned} \quad (\text{II-11})$$

Equations (II-6), (II-7), and (II-9) are a system of three partial differential equations with four unknowns; velocity components u , v , w , and pressure gradient $\frac{dp}{dr}$. Another equation is needed. Boyack [22] obtained this auxiliary equation by integrating equation (II-6) three times with respect to z and using the appropriate boundary conditions. The result is

$$\frac{dp}{dr} = - \frac{12 U_0}{N_{RE} r} + 24 \int_0^{1/2} \int_0^2 \int_0^\xi \left[\frac{u \partial u}{\partial r} + \frac{w \partial u}{\partial z} - \frac{v^2}{r} \right] d\beta \, d\xi \, dz \quad (\text{II-12})$$

where U_0 is the mean value of u_0 .

To produce the integral equation for the solution, equations (II-6), (II-7), and (II-9), are integrated over the interval $0 \leq z \leq 1/2$ and yield

$$\frac{1}{r} \frac{d}{dr} \left[r \int_0^{1/2} u^2 dz \right] - \int_0^{1/2} \frac{v^2}{r} dz = -\frac{1}{2} \frac{dp}{dr} + \frac{1}{N_{RE}} \frac{\partial u}{\partial z}(r, 1/2) \quad (\text{II-13})$$

$$\frac{1}{r^2} \frac{d}{dr} \left[r^2 \int_0^{1/2} u v dz \right] = \frac{1}{N_{RE}} \frac{\partial v}{\partial z}(r, 1/2) \quad (\text{II-14})$$

$$\int_0^{1/2} (r u) dz = \frac{U_0}{2r} \quad (\text{II-15})$$

Equations (II-12), (II-13), (II-14), and (II-15) constitute the integral equations Boyack uses in his investigation.

Nth order polynomial forms were chosen for the radial and tangential velocity profiles.

$$u(r, z) = \sum_{i=1}^{N+1} (a_{i-1}) z^{i-1} \quad (\text{II-16})$$

$$v(r, z) = \sum_{j=1}^{N+1} (b_{j-1}) z^{j-1} \quad (\text{II-17})$$

where a_i and b_j are functions of r . It follows that a representative for continuity be

$$w(r, z) = - \sum_{i=1}^{N+1} \left[\frac{a_{i-1}}{r} + a'_{i-1} \right] \frac{z^i}{i} \quad (\text{II-18})$$

where the prime denotes differentiation with respect to r .

Equations (II-16), (II-17), and (II-18) are substituted into the integral equations (II-12), (II-13), (II-14), and (II-15), to obtain

$$\frac{dp}{dr} = - \frac{12 U_0}{N_{RE} r} + 24 \sum_{i=1}^{N+1} \sum_{j=1}^{N+1} \frac{-Q_{i,j}}{(i+j-1)(i+j+1) 2^{(i+j+1)}} \quad (II-19)$$

where

$$Q_{i,j} = a_{i-1} a'_{j-1} - \frac{(j-1)}{i} a_{j-1} \left[\frac{a_{i-1}}{r} + a'_{i-1} \right] - \frac{b_{i-1} b_{j-1}}{r} \quad (II-20)$$

and

$$\sum_{i=1}^{N+1} \sum_{j=1}^{N+1} \frac{a_{i-1} a'_{j-1} + a'_{i-1} a_{j-1} + \frac{1}{r} (a_{i-1} a_{j-1} - b_{i-1} b_{j-1})}{(i+j-1) 2^{(i+j-1)}} + \frac{1}{2} \frac{dp}{dr} - \frac{1}{N_{RE}} \sum_{i=1}^{N+1} \frac{(i-1) a_{i-1}}{2^{(i-2)}} = 0 \quad (II-21)$$

$$\sum_{i=1}^{N+1} \sum_{j=1}^{N+1} \frac{a_{i-1} b'_{j-1} + a'_{i-1} b_{j-1} + \frac{2}{r} (a_{i-1} b_{j-1})}{(i+j-1) 2^{(i+j-1)}} - \frac{1}{N_{RE}} \sum_{i=1}^{N+1} \frac{(i-1) b_{i-1}}{2^{(i-2)}} \quad (II-22)$$

$$\sum_{i=1}^{N+1} \frac{a_{i-1}}{(i) 2^{(i)}} = \frac{U_0}{2r} \quad (II-23)$$

Matsch and Rice [25] found that highly inflected velocity profiles occur in the solution. To represent these profiles Boyack had to use polynomials of fourth and higher orders. The integral equations (II-19) through (II-23) and the boundary conditions are insufficient

to determine the coefficients a_i and b_i , so additional relations were needed. The additional relations between the a_i and b_i were obtained by requiring the differential forms of the momentum equations, (II-6) through (II-9), to be satisfied in the flow, and yield the correct number of equations to allow solutions for a_i and b_i .

The additional equations are

from (II-6)

$$\sum_{i=1}^{N+1} \sum_{j=1}^{N+1} \left[a_i a'_j - \left(\frac{a_i}{r} + a'_i \right) \frac{j a_j}{i+1} - \frac{b_i b_j}{r} \right] z^{i+j-2} + \frac{dp}{dr} - \frac{1}{N_{RE}} \sum_{i=1}^{N+1} (i-1)(i-2) a_i z^{i-3} = 0 \quad (\text{II-24})$$

from (II-7)

$$\sum_{i=1}^{N+1} \sum_{j=1}^{N+1} \left[a_i b'_j - \left(\frac{a_i}{r} + a'_i \right) \frac{j b_j}{i+1} - \frac{a_i b_j}{r} \right] z^{i+j-2} - \frac{1}{N_{RE}} \sum_{i=1}^{N+1} (i-1)(i-2) b_i z^{i-3} = 0 \quad (\text{II-25})$$

The coefficient of z^j is zero, so for every value of j , the compatibility relations are obtained from the above equations

$$a_0 a'_0 - \frac{b_0^2}{r} - \frac{2 a_2}{N_{RE}} + \frac{dp}{dr} = 0 \quad j = 0 \quad (\text{II-26})$$

$$\sum_{i=0}^j \left[a_i a'_{j-1} - \left(\frac{a_i}{r} + a'_i \right) \frac{(j-1)}{(i+1)} a_{j-1} - \frac{b_i b_{j-1}}{r} \right] - \frac{(j+1)(j+2)}{N_{RE}} a_{j+2} = 0 \quad j = 1, 2, \dots \quad (\text{II-27})$$

$$\sum_{i=0}^j \left[a_i b'_{j-1} - \left(\frac{a_i}{r} + a'_i \right) \frac{(j-1)}{(i+1)} b_{j-1} + \frac{a_i b_{j-1}}{r} \right] - \frac{(j+1)(j+2)}{N_{RE}} b_{j+2} = 0 \quad j = 0, 1, 2, \dots \quad (\text{II-28})$$

Using the boundary conditions on the radial and tangential velocity components at $z = 0$, Boyack simplified the compatibility equations, (II-27) and (II-28). From equations (II-27) the resulting equations are

$$a_2 a'_0 + a_0 a'_2 - \frac{2 b_0 b_2}{r} - 2 \left[\frac{a_0}{r} + a'_0 \right] a_2 - \frac{12 a_4}{N_{RE}} = 0 \quad (\text{II-29})$$

$$a_4 a'_0 + a_2 a'_2 + a_0 a'_4 - \frac{2 b_0 b_4}{r} - \frac{b_2^2}{r} - \frac{2}{3} \left[\frac{a_2}{r} + a'_2 \right] a_2 - 4 \left[\frac{a_0}{r} + a'_0 \right] a_4 - \frac{30 a_6}{N_{RE}} = 0 \quad (\text{II-30})$$

and from equations (II-28) the equations are

$$a_0 b'_0 + \frac{a_0 b_0}{r} - \frac{2 b_2}{N_{RE}} = 0 \quad (\text{II-31})$$

$$a_2 b'_0 + a_0 b'_2 + (a_0 b_2 + a_2 b_0) - 2 \left[\frac{a_0}{r} + a'_0 \right] b_2 - \frac{12 b_4}{N_{RE}} = 0 \quad (\text{II-32})$$

$$a_4 b'_0 + a_2 b'_2 + a_0 b'_4 + \frac{(a_4 b_0 + a_2 b_2 + a_0 b_4)}{r} - \frac{2}{3} \left[\frac{a_2}{r} + a'_2 \right] b_2 - 4 \left[\frac{a_0}{r} + a'_0 \right] b_4 - \frac{30 b_6}{N_{RE}} = 0 \quad (\text{II-33})$$

The equations Boyack used for the eighth order approximation to the exact solution are: the integral equations (II-21), (II-22), and (II-23), the simplified compatibility equations (II-29) through (II-33), and the boundary conditions which were not used in the previous derivations, $u(r, l/2) = 0$, and $v(r, l/2) = r$.

At the outer periphery of the disks, boundary conditions on a_i and b_i are required. If the values of a_i and b_i are specified at the inlet, this corresponds to specifying the distribution of $u_0(z)$ and $v_0(z)$. To obtain the initial values $a_i(1)$ and $b_i(1)$, Boyack fit to the inlet profiles a general polynomial representative for radial and tangential velocity components. The number of points which can be fit is pre-determined with the selection of either the fourth, sixth or eighth order approximation to the exact solution. The result is a system of linear, algebraic equations which can be solved for the unknown $a_i(1)$ and $b_i(1)$.

A numerical method was used by Boyack [22] to solve his simplified, initial value problem consisting of a system of ordinary differential equations and appropriate initial conditions. For each

radial step, Boyack found a solution could be obtained more efficiently by a predictor-corrector method. Although this method has very rapid computational time and the readily estimated error can be used as a basis for choosing step size, the solution must be known at r_{n-3} , r_{n-2} , r_{n-1} , and r_n in order to find the solutions at r_{n+1} . Thus the predictor-corrector method is not self-starting. For this reason, a Runge-Kutta-Gill method was used to provide the starting solution and an Adams-Moulton predictor-corrector method was used following the starting solution. These methods are well documented by Boyack [22].

Using a small step size the solution was started at $r = 1$. For each step forward the truncation error, E_K , was calculated and compared with preset allowable error limits, E_{\max} and E_{\min} . If $E_K > E_{\max}$ the step size was halved and the Runge-Kutta-Gill method was used to re-start the solution. If $E_K < E_{\min}$, the step size was doubled and the solution was re-started. If $E_{\min} < E_K < E_{\max}$, the step size remained constant and the A-M method was used to continue the calculation.

When comparing results for fourth, sixth and eighth order solutions with each other, Boyack found that the results for the fourth order solution were very poor due to the u velocity component becoming highly inflected at some radii. The results of the sixth and eighth order solution were in good agreement, indicating the solution approaches the correct solution as the order increases. Comparing the eighth order with the results obtained by Boyd [19] and Adams [21] the agreements were excellent. A complete outline of Boyack's digital computer program is given in Appendix A.

TURBINE PERFORMANCE PARAMETERS

A complete derivation of pertinent turbine performance parameters may be found in reference [19]. By taking a control volume consisting of the fluid between the disk inner and outer radii and applying a moment of momentum equation, the net torque on the turbine shaft is found. If all external rotor losses are neglected, the shaft torque is the negative of the control volume torque, and can be written as

$$T_s = 4\pi r_o^2 \int_0^{1/2} (u_o v_o) dz - 4\pi r_i^2 \int_0^{1/2} (u_i v_i) dz \quad (\text{II-34})$$

The total pressure is obtained from Bernoulli's equation and can be written as

$$p_t = p_o + \frac{1}{U_o} \int_0^{1/2} (u_o^2 + v_o^2) u_o dz \quad (\text{II-35})$$

The two above parameters can be expressed in terms of a_i and b_i if equations (II-16) and (II-17) are substituted into equations (II-34) and (II-35). As a result of the substitutions the following expressions are obtained

$$T_s = 4\pi \sum_{i=1}^{N+1} \sum_{j=1}^{N+1} \frac{(a_{oj} b_{oj} - r_i^2 a_i b_j)}{(i+j-1) 2^{(i+j-1)}} \quad (\text{II-36})$$

$$p_t = p_o + \frac{1}{U_o} \sum_{i=1}^{N+1} \sum_{j=1}^{N+1} \sum_{k=1}^{N+1} \frac{a_{oj} (a_{oj} a_{ok} + b_{oj} b_{ok})}{(i+j+k-2) 2^{(i+j+k-2)}} \quad (\text{II-37})$$

The efficiency of the turbine is expressed as the ratio of actual shaft work to the ideal shaft work, where the ideal shaft work is derived from the energy equation and the mass flow. The efficiency can be expressed as

$$\eta = \frac{T_s}{2\pi U_o p_t} \quad (\text{II-38})$$

Chapter III

PERFORMANCE MAPS

The primary objective of this study was to map the performance characteristics of the multiple-disk turbine. A designer can utilize the data shown in the maps to produce a wide variety of design charts in terms of dimensional quantities for a particular design study.

BOYACK'S COMPUTED RESULTS

For each combination of input parameters, U_0 , V_0 and N_{RE} a summary sheet is produced which tabulates the dimensionless turbine performance parameters total pressure (PT), pressure (P), torque (T), and efficiency (η) at specific radii R. In the summary R is the value of dimensionless inner radius of the turbine; therefore, the summary sheet covers an infinity of multiple-disk turbines. It was decided that the three dimensionless performance parameters, T, PT, and η could best describe the turbine characteristics. PT was chosen in lieu of P because P represents the pressure drop of the flow field within the disk region only. The value PT accounts for a pressure drop across the inlet nozzles as well as the disk region. The pressure drop across the nozzles does not remain constant; therefore the PT values provide a more adequate representation of the flow field.

Three different types of inlet velocity profiles can be assumed using the Boyack program, Matsch asymptotic, parabolic or uniform. The Matsch asymptotic profiles give results only applicable to the asymptotic flow region. The results obtained using parabolic and uniform velocity profiles are adequate to determine turbine characteristics because the solution of these profiles consider inlet conditions. It was decided to concentrate on the parabolic inlet profiles, because it is felt that the velocity profiles of the fluid exiting the stator nozzles is sufficiently developed to be parabolic in nature.

The Boyack program requires approximately 30 seconds to compute the performance parameters for a given combination of U_0 , V_0 and N_{RE} , using the CDC 6400 computer; making it extremely efficient as compared to the Boyd finite-difference method. A sample of the data summary sheets used in this study are presented in Appendix B.

It must be emphasized that all results presented are for a mathematical model having no losses external to the rotor. The model assumes perfect nozzles, perfect exhaust diffusion, no bearing or seal losses, and no windage losses between end disks and the rotor housing.

GRAPHICAL METHODS

The three performance parameters, η , T , and PT , were plotted as functions of U_0 and N_{RE} at specific radial locations and constant V_0 . To do this, a set of summary sheets was obtained and initial graphs were plotted. η , T , and PT versus U_0 were plotted separately with N_{RE} and V_0 constant at specific radial locations. Ten discrete, uniform radial locations were chosen, 0.1 to 0.9. The data from the

initial graphs was then cross-plotted to obtain constant value performance curves. To obtain these curves, constant values of η , T , and PT were taken from the initial graphs and plotted separately at corresponding values on a U_0 versus N_{RE} graph, with V_0 and R_i again constant. These points were later joined to form smooth and continuous curves of constant values for each of the nondimensional turbine parameters.

In a preliminary investigation of parabolic inlet profiles the input values for N_{RE} and U_0 were chosen as follows: $N_{RE} = 2.0, 4.0, 6.0, 8.0, \text{ and } 10.0$; $0.02 < U_0 < 1.0$, using an interval of 0.02 between 0.02 and 0.3, and an interval of 0.1 from 0.3 to 1.0. The value of $V_0 = 1.1$ was also used in the preliminary investigation. These points were selected to obtain, generally, the operating limits of the multiple-disk turbine. This initial investigation did indicate the operating limits and also areas which required further investigation.

It was found that for input values of U_0 greater than 0.3, at all N_{RE} values, efficiency was generally less than 20%, and total pressure extremely high, making this region of little interest in turbine design. The curves on the initial graphs were smooth and predictable, so it was decided that the narrow interval between the input values of U_0 could be relaxed. At lower values of N_{RE} it was found that η and PT undergo greater changes, and additional input values of N_{RE} had to be used to determine inflection points.

Using the preliminary investigation as a guide, further investigations of parabolic inlet profiles were conducted for input values of

$V_0 = 0.8, 1.0,$ and 1.3 . An investigation of uniform inlet profiles was also conducted for an input value of $V_0 = 1.1$.

Figures III-1 through III-3 are typical performance maps for constant values of dimensionless torque, total pressure, and efficiency. In addition composite maps were constructed, Figure III-4, which show a reduced number of curves superimposed on a single map for all three turbine parameters. These composite maps give a clearer understanding of the behavior of the turbine parameters with respect to each other. Complete sets of performance maps for parabolic inlet profiles with $V_0 = 1.0, 1.1,$ and 1.3 and uniform inlet profiles with $V_0 = 1.1$ are presented in Appendix C.

A large number of one-to-one graphs were plotted to verify the characteristics obtained on the performance maps. One set of graphs is constant value R_i curves plotted for corresponding η , T , or PT and V_0 with U_0 and N_{RE} constant. The other set of one-to-one graphs is constant value N_{RE} curves plotted for corresponding η and R_i with U_0 and V_0 constant. A selected number of these curves are in Appendix C.

GENERAL CURVE CHARACTERISTICS

Looking at the performance maps for a fixed V_0 , it is evident that η increases as R_i and U_0 decrease. The dimensionless torque T increases as R_i decreases and it decreases as U_0 decreases. PT the dimensionless total pressure decreases as U_0 decreases and it increases as R_i decreases. In the region of the maps where U_0 is greater than 0.10 , efficiency is low; total pressure and torque are high. Here the performance maps indicate that high torque turbines are possible at

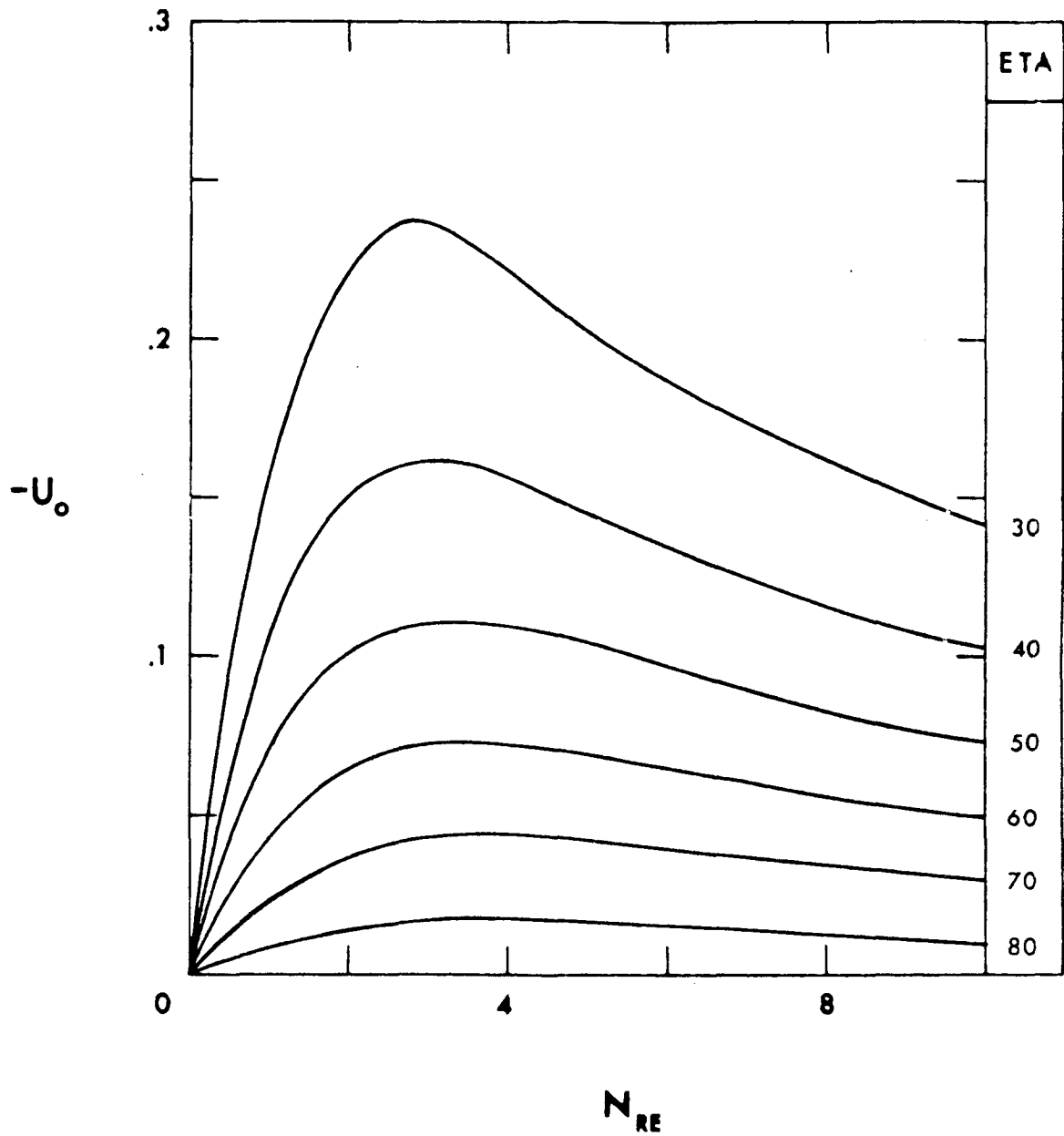


Figure III-1. Typical Map of Turbine Efficiency as a Function of U_0 and N_{RE} for $V_0 = 1.1$, $R_j = 0.3$ and Parabolic Inlet

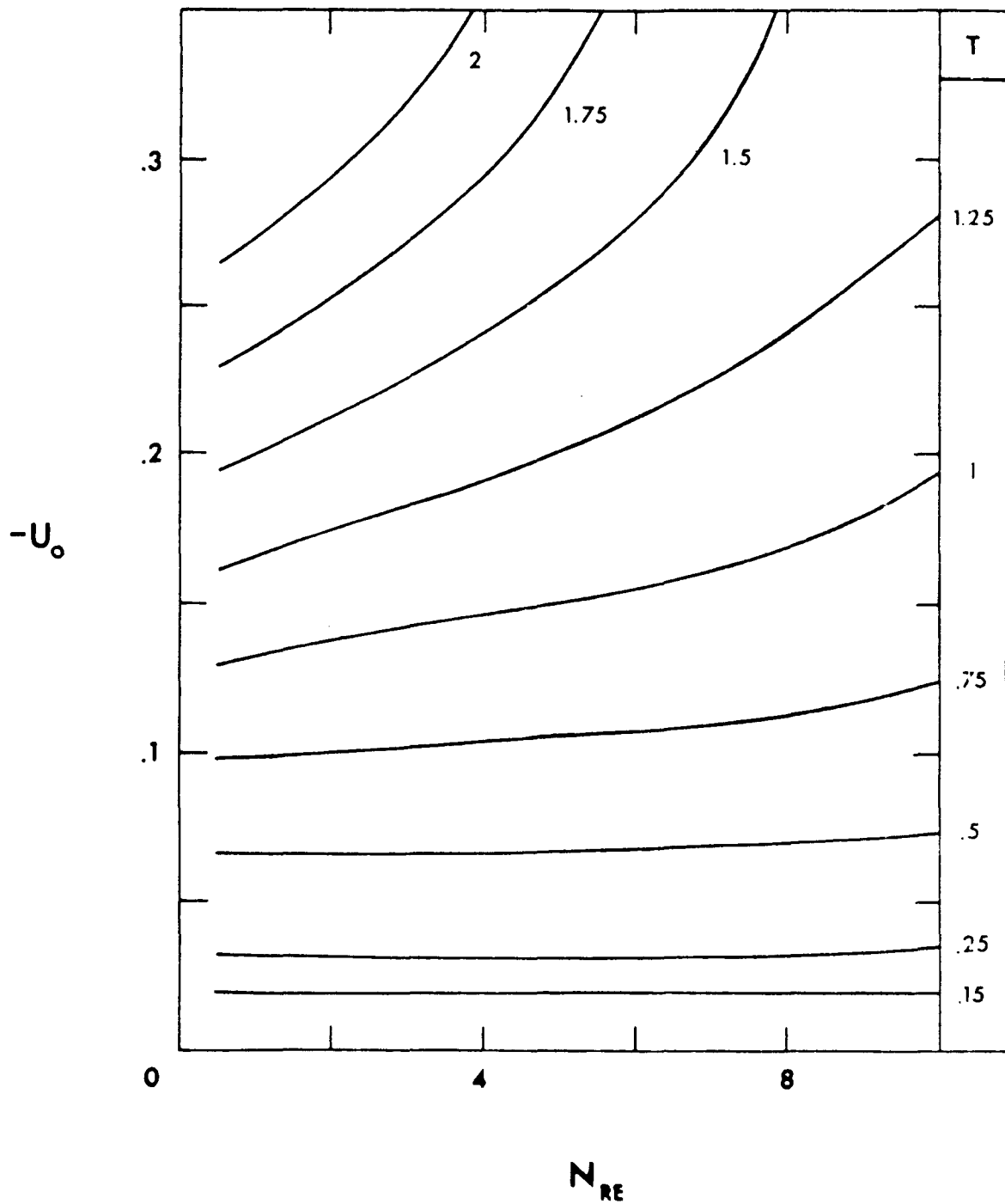


Figure III-2. Typical Map of Turbine Dimensionless Torque as a Function of U_0 and N_{RE} for $V_0 = 1.1$, $R_i = 0.3$ and Parabolic Inlet

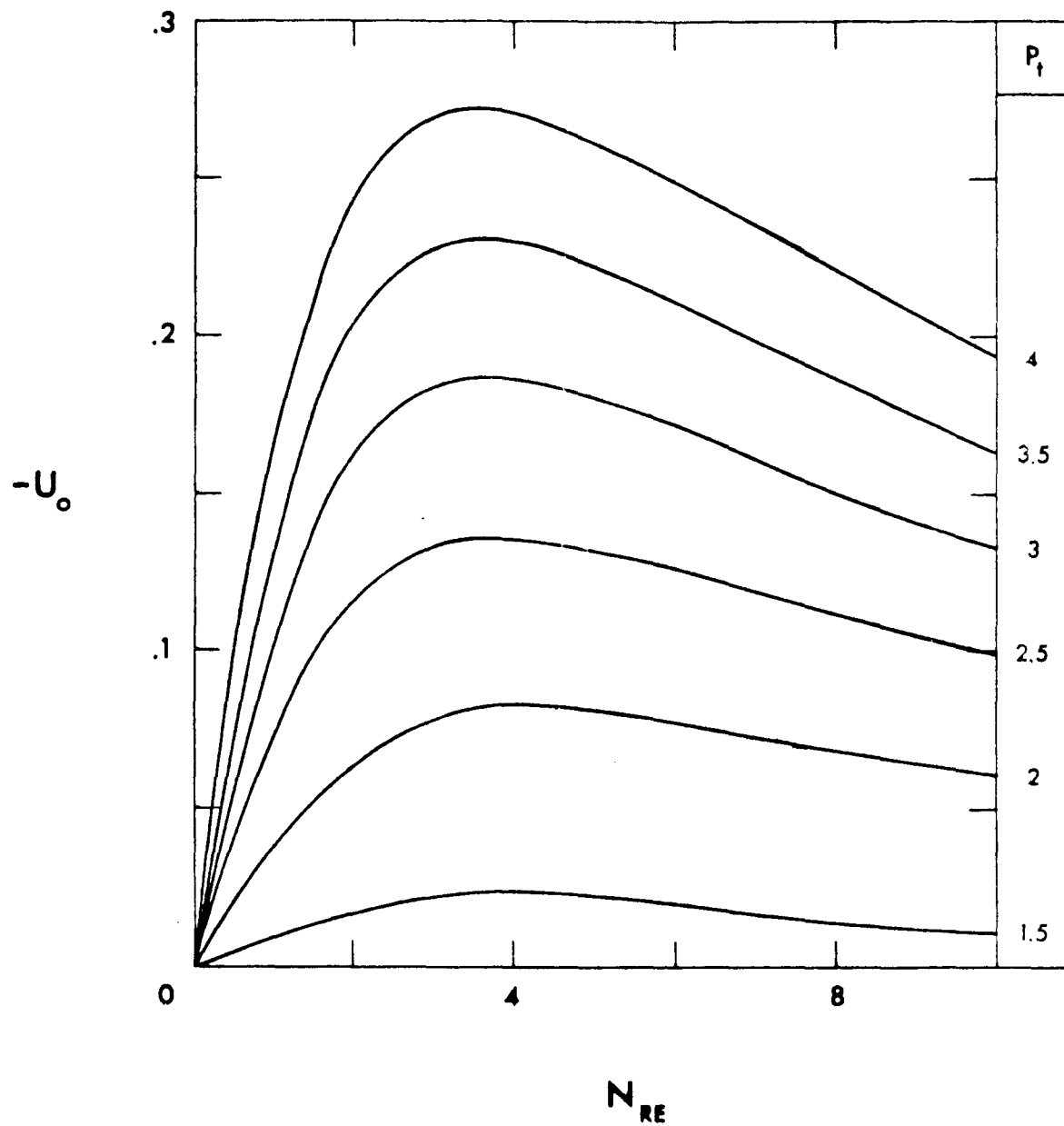


Figure III-3. Typical Map of Turbine Dimensionless Total Pressure as a Function of U_0 and N_{RE} , for $V_0 = 1.1$, $R_i = 0.3$ and Parabolic Inlet

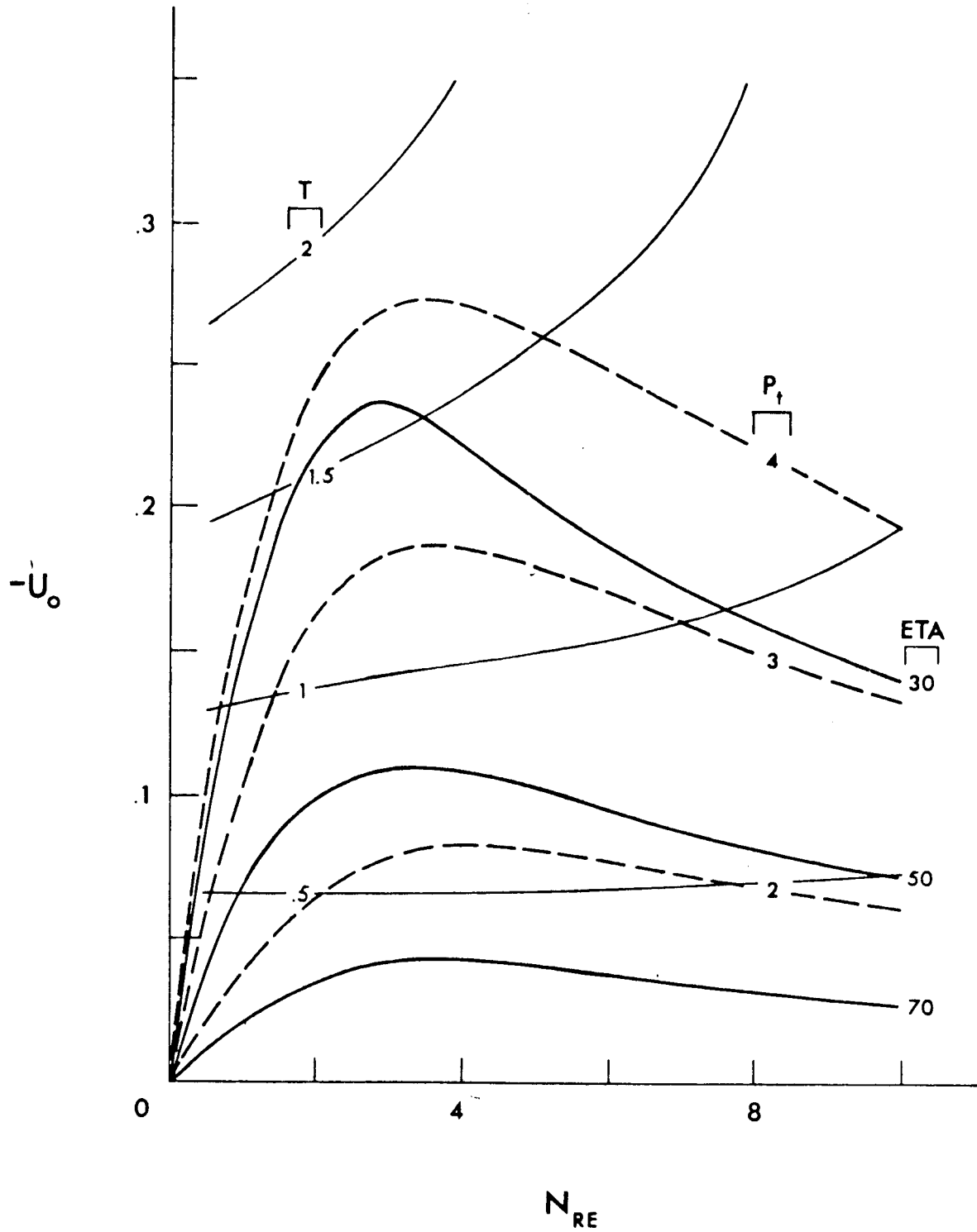


Figure III-4. Composite Map Showing η , T , and PT as a Function of U_0 and N_{RE} for $V_0 = 1.1$, $R_i = 0.3$ and Parabolic Inlet

the expense of low efficiency and high total pressure. This region of operation has questionable utility.

The area of prime interest lies in the region where U_0 is less than 0.05. Through the range of N_{RE} , the T curves have relatively zero slope for any given U_0 . The PT curves in this region do not have drastic inflections and their values are small. It follows that at a particular value of U_0 , η is a function of PT only since

$$\eta = \frac{T}{2\pi U_0 PT} \quad (\text{III-1})$$

As previously stated T decreases as U_0 decreases so this region is ideal for the design of small, low powered turbines, because high efficiency and low total pressure requirements are easily obtained.

If a particular value of torque is required, it is possible to choose from the performance maps a design value for the exhaust radius that will provide maximum efficiency; or if a specific total pressure drop is available the exhaust radius can be picked to provide maximum efficiency, and the corresponding values of U_0 and N_{RE} are fixed. There are any number of combinations available.

The first set of one-to-one plots (η versus V_0), verify that efficiency increases as R_i decreases to a value of about 0.3; then the efficiency starts to decrease. The maximum efficiency occurs within one-tenth of $V_0 = 1.0$. The other two parameter graphs indicate the values of PT and T decreases as R_i increases for all V_0 .

The other set of one-to-one plots (η versus R_i) shows that the efficiency peaks at R_i equal to about 0.3 and $N_{RE} = 4.0$ for all U_0 and V_0 .

The performance maps for the uniform inlet profiles follow the same pattern as the ones for the parabolic inlet profiles. During the investigation it was found that the polynomial representation for uniform inlet profiles presented in reference [22] was incorrect. A suitable representation, which could be solved by the Boyack integral method, was not found. Crawford [29], during his analytical design and optimization study of a multiple-disk pump, developed a method using the Boyd [19] finite-difference technique to obtain a solution in the entrance region. When the velocity profiles can be represented by a polynomial, without discontinuities, the Boyack integral method is used to continue the solution. The profile match-up occurs before the flow reaches $R_i = 0.98$ and generally takes 60 finite-difference steps.

The area of interest on the performance maps for the uniform inlet profiles is the region where the input values of U_0 are less than 0.06. The scale of the maps was changed to show only this region. While the patterns of the curves remain the same as the parabolic inlet profiles, the values of the parameters change significantly. The efficiency increases approximately 10%, while the total pressure decreases and the torque remains about the same for a given U_0 .

LIMITATIONS

The investigation of the multiple-disk turbine performance parameters disclosed that the turbine was limited in three areas. The first

occurs when the inlet profiles are parabolic and the input parameters are $U_0 < 0.02$, $N_{RE} > 4.0$, and all V_0 . In this region Crawford discovered that the velocity profiles collapsed, recovering for some cases, but not for others. This explains the discontinuity indicated on the performance maps for parabolic inlet profiles with $V_0 = 1.3$. As N_{RE} becomes larger with $U_0 < 0.02$, the velocity profiles show that the flow between the disks becomes reversed and high shear forces prevent the fluid from continuing inward.

The other two limitations are generally impractical. First is the combination of input parameters, $U_0 > 1.0$, all N_{RE} , and all V_0 . The efficiency remains extremely low and the total pressure drop required to turn the turbine is extremely high. In some cases the efficiency remains negative, a finite distance beyond the entrance region, indicating a pumping action.

The other impractical area is the combination of input parameters, $V_0 < 1.0$, all U_0 , and all N_{RE} . V_0 is defined as the mean value of $v(1,z)$ and

$$v(1,z) = \frac{\bar{v}}{\bar{r}_0 \Omega} \quad (\text{III-2})$$

If $v_0(z)$ is less than 1.0, the initial tangential velocity of the fluid must be less than the tangential velocity of the outer periphery of the disks. The disks must do work on the fluid to bring its velocity up to velocity of the disks, and is so indicated in the data summary sheets as a negative efficiency. The velocity of the fluid attains the velocity of the disks before the flow reaches $R_i = 0.95$, but not before a finite amount of turbine shaft work is lost.

While the operation of the multiple-disk turbine in the regions described above seem to have little utility, there may be special situations where operating in these areas may be useful.

DESIGN CHARACTERISTICS

A turbine designer can approach a design problem in many ways. Physical constraints and operating conditions dictate which approach to design must be taken. The performance maps presented in Appendix C are beneficial in visualizing the dependence of η , T , and PT on N_{RE} , U_0 , V_0 , and R_i . Using the maps, a number of design charts in terms of dimensional quantities can be produced for a particular study. The problem depends on parameters which are fixed, known and unknown. The result can be one of a large number of possible combinations of input and output data.

Presented is an example of an initial design study of a multiple-disk turbine rotor. The first step is to dimensionalize the performance map parameters. From reference [19] the following equations for the dimensionless parameters are obtained.

$$PT = \frac{\bar{PT}}{\rho \Omega^2 \bar{r}_0^2} \quad (\text{III-3})$$

$$T = \frac{\bar{T}}{\rho \bar{r}_0^4 \Omega^2 \bar{h}} \quad (\text{III-4})$$

$$\eta = \frac{T}{2\pi U_0 PT} \quad (\text{III-1})$$

$$N_{RE} = \frac{\bar{h}^2 \Omega}{\nu} \quad (\text{III-5})$$

Solving equations (III-3) and (III-4) for dimensional total pressure and torque the following is obtained.

$$\bar{PT} = PT \rho \Omega^2 \bar{r}_0^2 \quad (\text{III-6})$$

and
$$\bar{T} = T \rho \bar{r}_0^4 \Omega^2 \bar{h} \quad (\text{III-7})$$

Using equations (III-3) to obtain the angular velocity gives

$$\Omega = \left(\frac{\bar{PT}}{PT \rho \bar{r}_0^2} \right)^{1/2} \quad (\text{III-8})$$

In reference [22] a form of the integrated continuity equations at the outer radius is

$$Q = 2\pi \Omega \bar{h} U_0 \bar{r}_0^2 \quad (\text{III-9})$$

where Q is the volume flow rate. With the above equations η can now be presented as a function of dimensional parameters.

$$\eta = \frac{\bar{T} \Omega}{Q \bar{PT}} \quad (\text{III-10})$$

Solving equations (III-5) for \bar{h} , the disk spacing, yields

$$\bar{h} = \left(\frac{N_{RE} \nu}{\Omega} \right)^{1/2} \quad (\text{III-11})$$

Finally the inlet nozzle angle α is defined as

$$\alpha = \tan^{-1} \frac{U_0}{V_0} \quad (\text{III-12})$$

All turbine parameters are now in terms of dimensional quantities.

A digital computer program was developed to use the input and output results of the modified Boyack program with the dimensional total pressure (head) and outer rotor radius available as additional input data. The program outputs are the dimensional quantities needed for initial design studies. In addition the program computes off design point conditions caused by a varying head. A listing of the design program is presented in Appendix D.

In an example presented herein it is assumed that efficiency must be at least 80%, the maximum head available is 220 feet, and the velocity inlet profiles are parabolic. From the performance maps it is seen that efficiency approaches 80% in the region where $R_i = 0.3$, $U_o = 0.02$, $V_o = 1.1$, and $N_{RE} = 4.0$. The data summary sheets indicate that with those input parameters the output characteristics are $\eta = 79.5$, $PT = 1.525$, and $T = 0.152$. Using the above nondimensional parameters, fixing the disk thickness and rotor length-to-radius ratio, the dimensional characteristics were calculated for a given working fluid.

Using liquid hydrogen, liquid sodium, and glycerin, and assuming they behave as incompressible Newtonian fluids, the dimensional operating characteristics of a multiple-disk rotor were studied. Figure III-5 shows how the design angular velocity (RPM) of the rotor and output torque (FT-LB) vary as the fluid density varies with selected outer radii. As the fluid density and outer radius increase the RPM decreases while the torque increases at design conditions. High power outputs occur in large rotors using dense fluids.

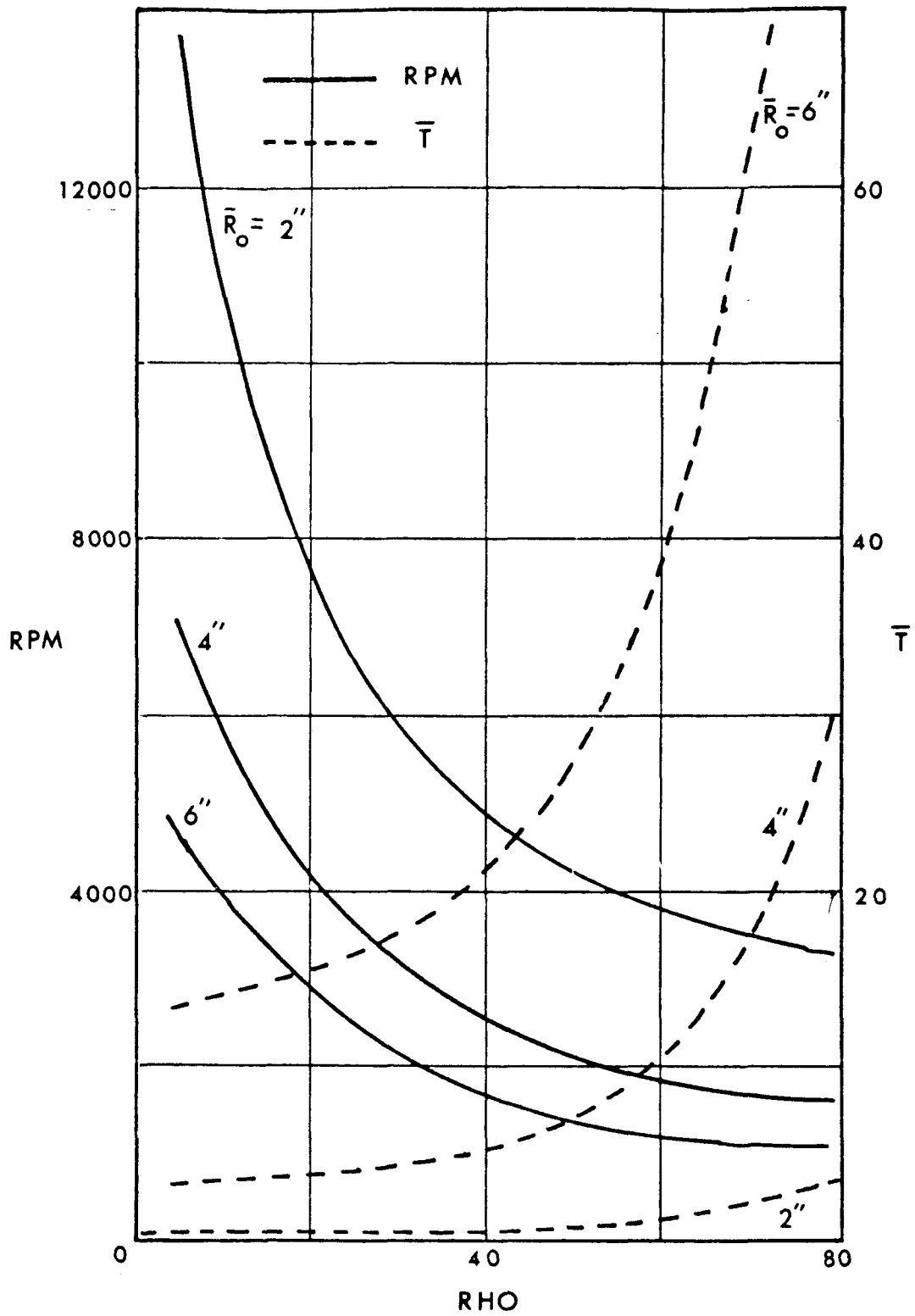


Figure III-5. Plot of RPM and Torque Versus Density with Head = 200 Feet

The graphs in Figures III-6 through III-8 illustrate how the design angular velocity, torque, and disk spacing (inches) vary as the design head varies for a given rotor size. When the design head increases, the disk spacing becomes narrower, so for a given size rotor the number of disks must increase to meet the design characteristics. Denser fluids require wider disk spacing, and a lesser number of disks. The torque and angular velocity increase as the design head increases, and it follows that the output power increases. For a fixed size rotor, the increase of the design head produces an increased volume flow.

Figures III-9 through III-11 show how design angular velocity, disk spacing, and torque vary as the design rotor size varies for a given head. Here again it is evident that larger rotors require wider disk spacing and produce higher torque. From equations (III-9) Q is a function of Ω , \bar{h} , and \bar{r}_0^2 . Therefore, in large rotors volume flow becomes significant.

The figures described above were for design conditions for the various parameters mentioned. Figures III-12 through III-14 illustrate a typical off-design-point operation. For a given design the fluid design head was allowed to vary $\pm 20\%$. The efficiency of the off design operation was calculated using equation (III-10), and did not vary. The torque and the power varied $\pm 20\%$ and $\pm 30\%$ respectively. The volume flow, however, only varied $\pm 10\%$. The above percent changes are independent of rotor size and working fluid.

The study presented is an example of how a design problem can be approached. For a specific turbine requirement there are numerous combinations of parameters which can be varied to obtain an optimum design.

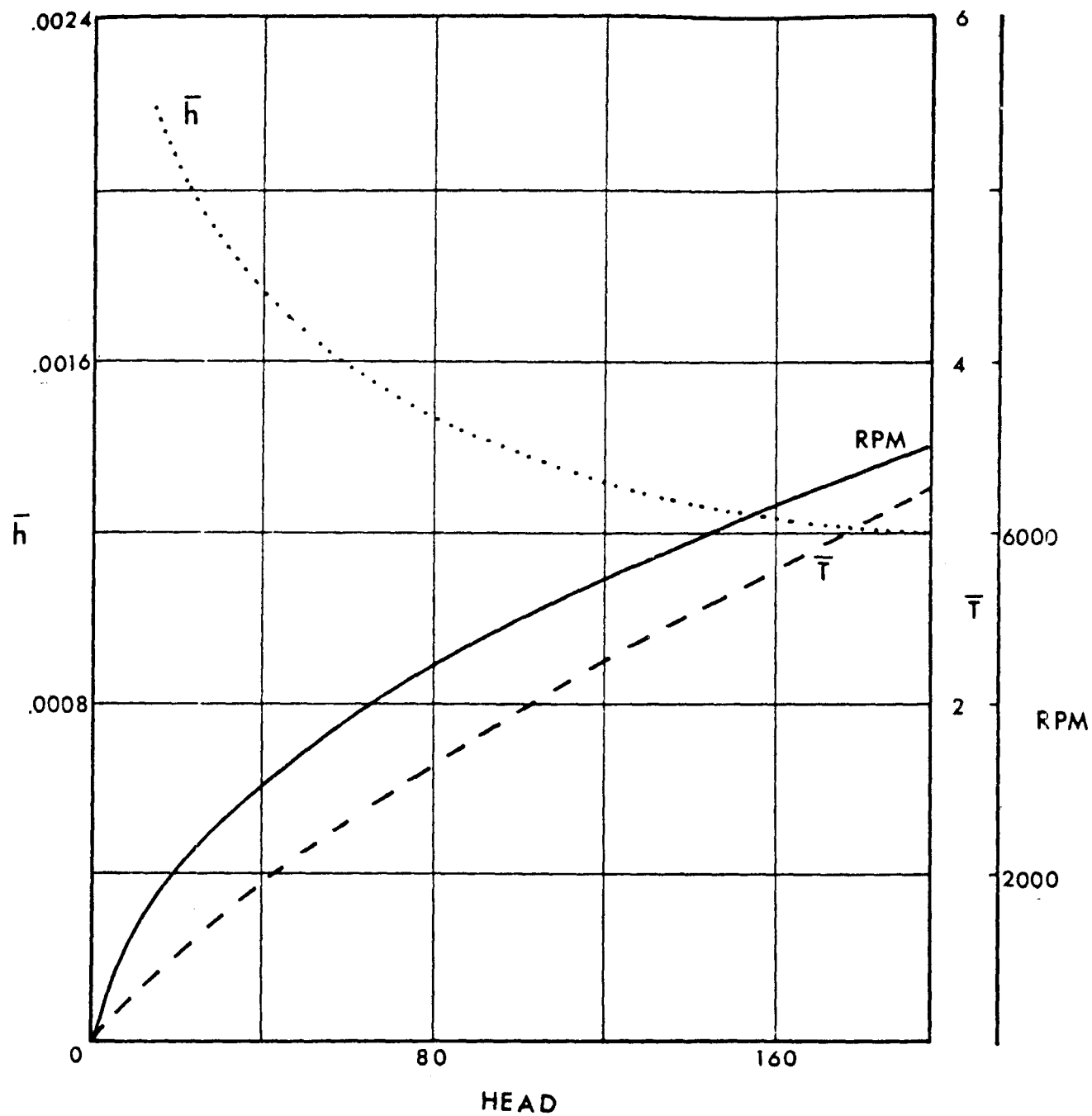


Figure III-6. Plot of RPM, Disk Spacing, and Torque Versus Head for Liquid Hydrogen and Outer Rotor Radius = 4.0 Inches

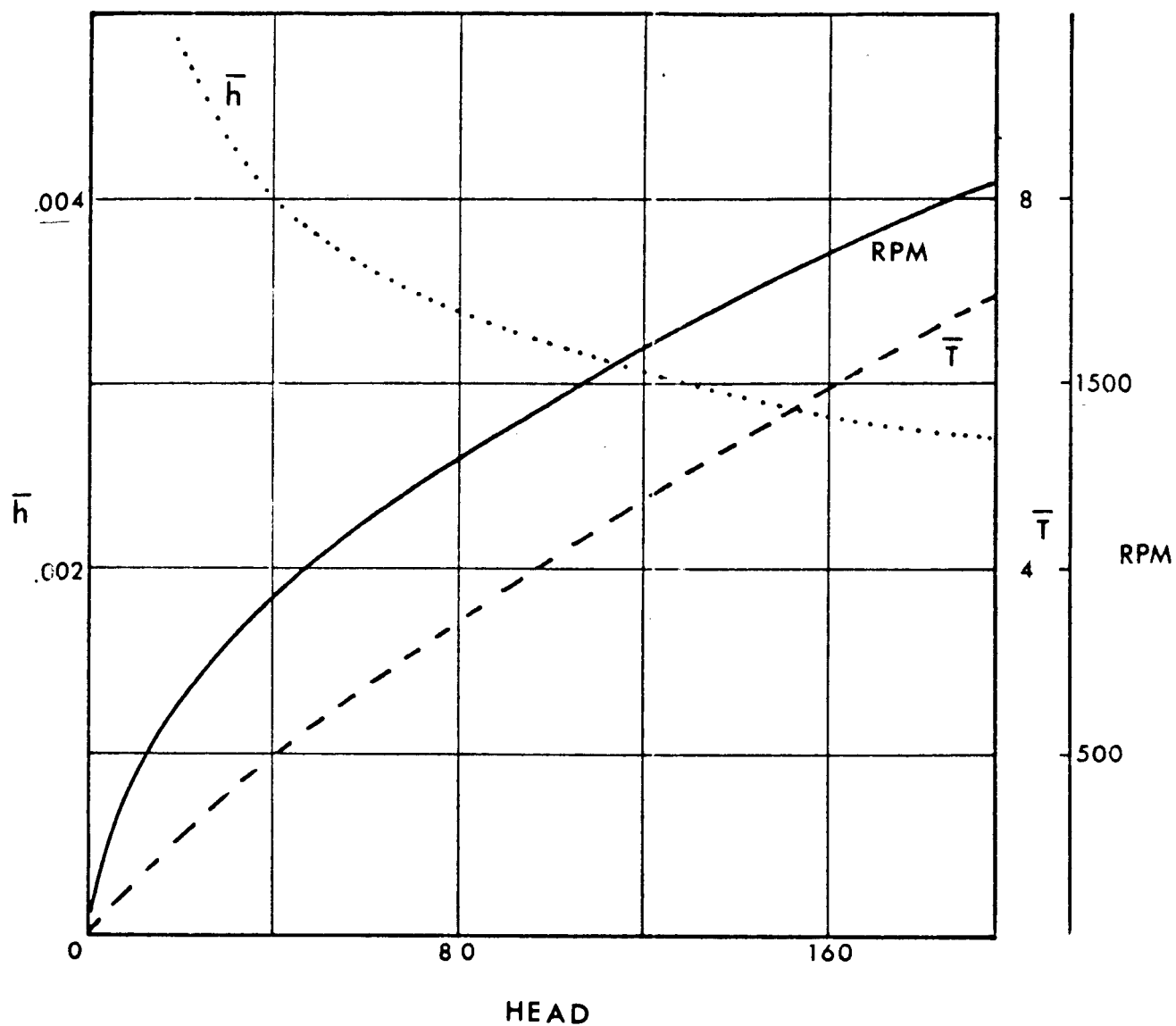


Figure III-7. Plot of RPM, Disk Spacing, and Torque Versus Head for Liquid Sodium and Outer Rotor Radius = 4.0 Inches

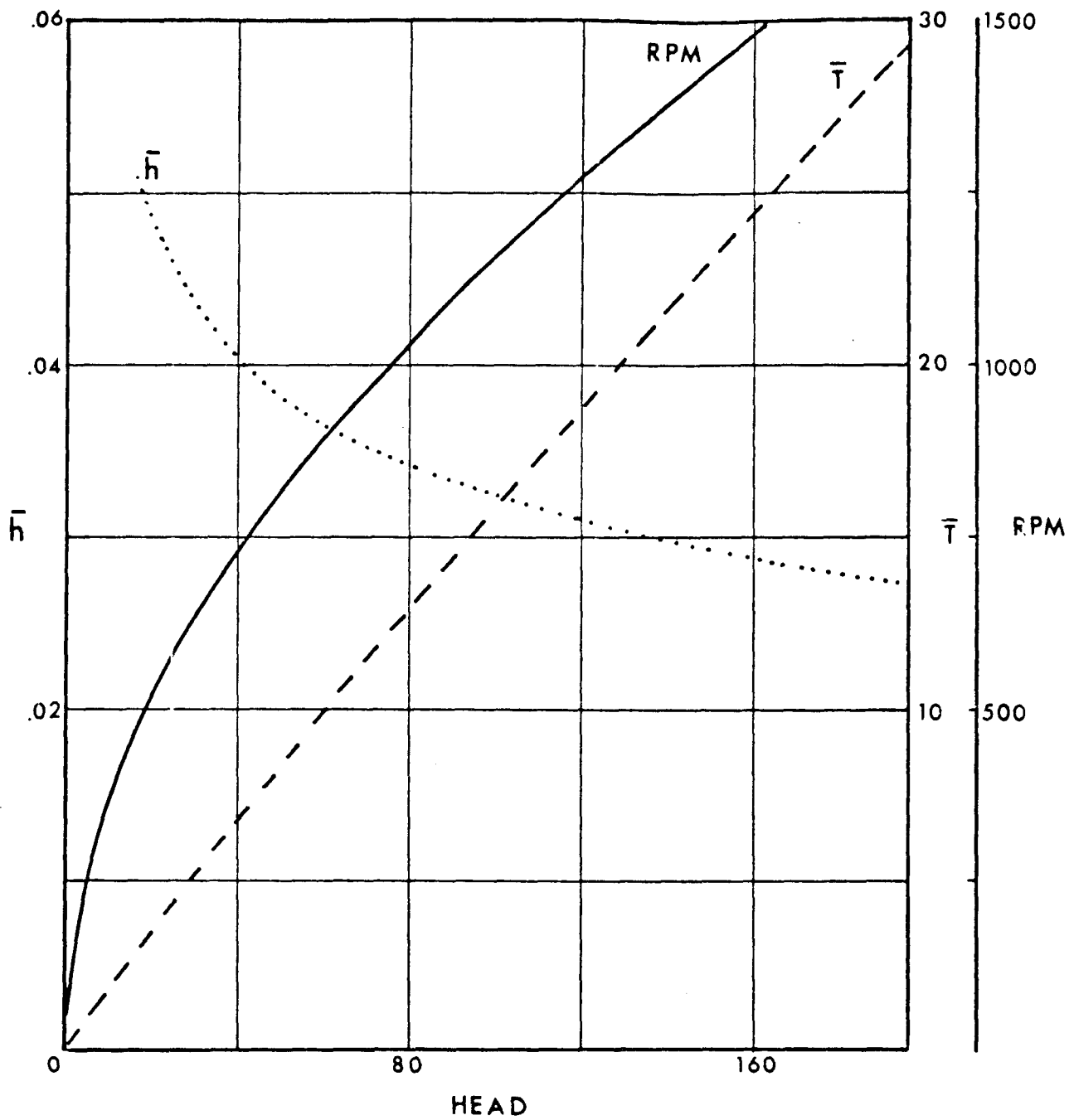


Figure III-8. Plot of RPM, Disk Spacing, and Torque Versus Head for Glycerine and Outer Rotor Radius = 4.0 Inches